High-temperature stability, pyrolysis kinetics and mechanism between bio-based and petro-based resins using TG-FTIR/MS

Dan Zhou, Xiaopeng Chen, Jiezhen Liang, Xiaojie Wei,

Chenghong Wu, Wenhui Li, Linlin Wang*

School of Chemistry and Chemical Engineering, Guangxi Key Laboratory of Petrochemical Resources Processing and Process Intensification Technology, Guangxi University, Nanning 530004, PR China

ABSTRACT

Pyrolysis behavior of bio-based resins is of increasing interest due to their great potential in environmentally friendly and high-temperature application. Herein, the high-temperature stability, pyrolysis kinetics and mechanism of rosin glyceride (RGE), hydrogenated rosin glyceride (HRGE), C9 petro-based resin (C9PR) and hydrogenated C9 petro-based resin (HC9PR) under non-oxidizing atmosphere were investigated by TG-FTIR/MS techniques. Based on the non-isothermal TG data, activation energy was calculated by Friedman and Starink methods, and the reaction-order model of $f(\alpha)=(1-\alpha)^n$ was found to be the most probable pyrolysis mechanism for different resins, which was also supported by the TG-FTIR/MS results showing only a dominating pyrolysis peak. Furthermore, thanks to the unique tricyclic phenanthrene structures, bio-based resins exhibit better high-temperature stability than petro-based resins, with an initial skeleton cracking temperature of 623 K and

*Corresponding author. Tel.: +86–771–3272702; fax: +86–771–323–3718

E–mail address: wanglinlin1971@sina.com.

573 K, respectively. High-temperature stability of resins would mildly decrease after hydromodification due to weak bonds cracking. Possible pyrolysis pathways were proposed.

Keywords: bio-based resin, petro-based resin, high-temperature stability, pyrolysis mechanism, kinetics

1. Introduction

Energy crisis and pollution are growing problems in the world due to the vast consumption of petrochemical resources.[1-2] Renewable biological energy is of increasing interest, which can replace traditional petro-based resources for the synthesis of useful fine chemicals and polymeric materials and reduce environmental pollution.[1-4]

Thermoplastic resins are widely applied in adhesives, hot melts, printing inks, coatings, varnishes, rubber tires, sealants and floor tiles due to their excellent weatherability, light aging resistance, high-temperature stability, adhesiveness and miscibility.[5-7] C9 petro-based resin (C9PR), which is typically synthesized by the polymerization of C9 fraction (such as indene, methylstyrene, α-methylstyrene, dicyclopentadiene and so on) derived from the ethylene cracking in the petroleum industry, is one of the most important petro-based thermoplastic resins and possess good high-temperature stability and high mechanical property due to the high cycloaliphatic or aromatic content.[5,7-8] hydrogenated C9 petro-based resin (HC9PR) with high oxidation stability and light color is obtained by hydrogenation of C9PR and it shows higher application value than C9PR, which is due to the fact that the

C9PR is rich in unsaturated bonds, especially ethylenic C=C bond, and easy to be oxidized in the air, resulting in darker color, poor oxidation stability, poor adhesiveness and poor compatibility.[9-11] Despite a good property, the application of C9PR and HC9PR in food and pharmaceutical additives is banned since the hazard for human health, such as strong carcinogenic naphthalene and indene.[10,12] In addition, the continuous use of petro-based resins may result in great consumption of petrochemical resources. Considering the energy and health problems caused by petro-based thermoplastic resins, there is a requirement to develop an environmentally friendly and renewable biological resources for the synthesis of bio-based thermoplastic resins.

Rosin glyceride (RGE) and hydrogenated rosin glyceride (HRGE) have become promising alternatives to petro-based resins due to their renewable, environmentally friendly, non-toxic and readily biodegradable properties, which are widely used in chewing gum base, plasters and drug film coating, ect.[13-15] RGE and HRGE are bio-based thermoplastic resins synthesized by the esterification of glycerol with rosin or hydrogenated rosin.[13,16] Rosin is an abundantly renewable resin that is obtained naturally from the exudations of pines and conifers or from the tall oil as a byproduct of paper pulp production, and made up of 90% tricyclic phenanthrene resin acids and 10% neutral compounds[13-18]. Similar to C9PR, rosin has conjugated double bonds which are easily oxidized to reduce product quality, thus hydrogenation modification of rosin or RGE is carried out, and then the HRGE with light color and high oxidation stability is synthesized.[16,19-20] RGE and HRGE have similar rigidity to petro-based

resins due to their large tricyclic phenanthrene structure.[14,17] Typically, adhesiveness, compatibility, color, oxidation stability and high-temperature stability are important characteristics for industrial applications of bio-based and petro-based resins.[5,9-10,21-24] In terms of compatible and adhesive properties, the application of RGE or HRGE as a substitute for petro-based resins has been reported, such as hot melt adhesives,[21,25] and pressure-sensitive adhesives.[22,26] Besides, based on the color and antioxidant properties, many researchers have focused on the hydrogenation of bio-based and petro-based resins.[9-11,27] Although some studies concerning the high-temperature stability and pyrolysis kinetics of rosin or dicyclopentadiene resins have been carried out,[23-24] the study on the high-temperature stability comparison between bio-based and petro-based resins is still absent. In addition, to the best of our knowledge, no information on the pyrolysis kinetics and mechanism of RGE, HRGE, C9PR and HC9PR is available in the open literature.

High-temperature stability of thermoplastic resins is an essential characteristics for their high-temperature applications.[20,23-24] bio-based and petro-based resins are usually used in a wide range of temperatures, such as thermoplastic road-marking paints[28] and asphalt,[6] as a result, whether bio-based resins can replace petro-based resins has an important relationship with their high-temperature stability. Therefore, it is necessary to investigate the high-temperature stability, pyrolysis kinetics and mechanism of bio-based and petro-based resins under non-oxidizing atmosphere.

Thermogravimentric analysis (TG) is the most common method to investigate the high-temperature stability and pyrolysis kinetics of solids.[2,20,29-30] The model-free

and model-fitting methods are widely employed to estimate the kinetic parameters using TG and differential thermograwimetric (DTG) curves with different heating rates.[2,30-34] The isoconversional model-free methods could evaluate the activation energy ($E\alpha$) without determining the reaction mechanism.[30-34] Generally, the integral and differential isoconversional methods (such as Friedman and Starink) were used to estimate the $E\alpha$, which allowed for meaningful mechanistic analyses and reliable kinetic predictions.[30-34] The model-fitting methods with single-step or multi-step models are usually employed to investigate the pyrolysis kinetics and mechanism.[30-33] Furthermore, thermogravimetry coupled with fourier transform infrared spectrometer or mass spectrometry (TG-FTIR/MS) techniques could be adopted to identify the gasous products released from the pyrolysis process and better understand the pyrolysis mechanism.[2,8,20,29]

Accordingly, this study aims to investigate the high-temperature stability, pyrolysis kinetics and mechanism of RGE, HRGE, C9PR and HC9PR under non-oxidizing atmosphere using TG-FTIR/MS techniques. The model-free and model-fitting methods were employed to explore the pyrolysis kinetics and mechanism of bio-based and petro-based resins based on the non-isothermal TG data, in which the activation energy was calculated by Friedman and Starink methods and the mechanism function was determined by the reaction-order and Sestak-Berggren models. Moreover, the high-temperature stability of bio-based and petro-based resins before and after hydrotreating was evaluated and compared according to the kinetic and TG-FTIR/MS analyses. Finally, detail pyrolysis gaseous products information

were identified based on the TG-FTIR/MS analyses, and the possible pyrolysis pathways of bio-based and petro-based resins were proposed.

2. Materials and methods

2.1 Materials

RGE and HRGE were purchased from Guangxi Wuzhou Pine Chemicals Co., Ltd. C9PR was supplied by PetroChina Lanzhou Huifeng Petrochemical Co., Ltd. No, and the corresponding HC9PR was prepared according to the previous work of our research group.[11] All materials were used to evaluate their pyrolysis behaviors without further purification and pretreatment.

2.2 *Experimental tests*

To examine the pyrolysis behaviour of RGE, HRGE, C9PR and HC9PR, TG experiments were carried out in a thermal analyser (TG 209 F3 Tarsus®, NETZSCH, Germany) at the heating rates of 5, 10, 20 and 40 $K \cdot min^{-1}$ with a nitrogen flow rate of 40 $mL \cdot min^{-1}$. The sample with a mass of 6.5 ± 0.4 mg was used in each test, and the heating temperature was increased from ambient to 873 K. Furthermore, to identify the pyrolysis gaseous products and better understand the pyrolysis mechanism, both TG-FTIR (Thermo is50 METTLER TG2, USA) and TG-MS (thermo plus EV2/ thermo mass photo, USA) was conducted in a helium gas with a heating rate of 10 $K \cdot min^{-1}$. The molecular weight distributions of samples were measured by gel permeation chromatography (GPC, SHIMADZU, RID-20a, Japan).

2.3 Kinetic modeling

The high-temperature stability of bio-based and petro-based resins is an

important characteristics to determine their industrial application and life.[5,20] To explore the high-temperature stability and pyrolysis kinetics and mechanism of bio-based and petro-based resins, it is necessary to develop a pyrolysis kinetic model. The kinetic equations can be expressed as:

$$\frac{d\alpha}{dt} = kf(\alpha) \tag{1}$$

$$\alpha = \frac{m_0 - m_t}{m_0 - m_f} \tag{2}$$

Where $f(\alpha)$ is the function of the reaction mechanism, α is the degree of conversion, t is reaction time and m_0, m_t and m_f is the initial, t time and end masses of samples, respectively. k is the reaction rate constant, usually described by Arrhenius equation as:

$$k = A\exp(-\frac{E_\alpha}{RT}) \tag{3}$$

Where A is the pre-exponential factor, min^{-1}; E_α is the activation energy of the pyrolysis reaction, kJ/mol and T is the temperature, K.

For non-isothermal measurements with a linear heating rate, $\beta = dT/dt$, combining Eqs.(1) and (3) yielded the Eq.(4) as following:

$$\frac{d\alpha}{dT} = \frac{A}{\beta}\cdot\exp(-\frac{E_\alpha}{RT})f(\alpha) \tag{4}$$

The integration of Eq.(4) under the initial conditions (α =0, at T=T_0) is expressed as:

$$g(\alpha) = \int_0^\alpha \frac{d\alpha}{f(\alpha)} = \frac{A}{\beta}\int_{T_0}^{T}\exp(-\frac{E_\alpha}{RT})dT \tag{5}$$

Regarding kinetic model determining, the isoconversional model-free and

model-fitting methods were used to evaluate the pyrolysis kinetic parameters based on the non-isothermal TG data.[2,30-34] The most common differential and integral isoconversional methods to evaluate the activation energy are Friedman and Starink methods, respectively.[31,34] Friedman method can be expressed based on the following equation:

$$\ln \beta(\frac{d\alpha}{dT}) = \ln[f(\alpha)A] - \frac{E_\alpha}{RT} \quad (6)$$

In this method, the reaction mechanism function $f(\alpha)$ remains constant, and the value of E_α is determined from the slope of a plot $\ln(\beta d\alpha/(dT))$ vs $1/T$.

In the Starink method,[31] the resultant equation was written below:

$$\ln(\frac{\beta}{T^{1.92}}) = const - 1.0008(\frac{E_\alpha}{RT}) \quad (7)$$

From Eq.(7), the value of E_α is determined from the slope of a plot $\ln(\beta/T^{1.92})$ vs $1/T$.

In this work, the model-fitting methods with single-step model was assumed to determine the pyrolysis kinetics and mechanism of bio-based and petro-based resins.[30-31,33] Usually, the reaction-order (*n*th order) model was considered to describe the reaction mechanism of single-step model for solid-state reactions.[2,30,33,36] The *n*th order model is expressed by the following equation:

$$f(\alpha) = (1-\alpha)^n \quad (8)$$

Hence, Eq.(4) can be rewritten as

$$\frac{d\alpha}{dT} = \frac{A}{\beta} \cdot \exp(-\frac{E_\alpha}{RT})(1-\alpha)^n \quad (9)$$

Besides, a modified form of the truncated empirical model by Sestak-Berggren (TSB)[30-31] was also proposed to describe the reaction mechanism of single-step model,

and it can be described as

$$f(\alpha) = c(1-\alpha)^n \alpha^m \tag{10}$$

Combing Eqs.(4) and (10) yields:

$$\frac{d\alpha}{dT} = \frac{A}{\beta} \cdot \exp(-\frac{E_\alpha}{RT})(1-\alpha)^n \alpha^m \tag{11}$$

Where *n* and *m* are empirical fitting parameters, representing the reaction order and accelerating mechanisms, respectively. The TSB model is a combined model, which depends on the combination of *n* and *m* can elucidate the possible reaction mechanisms.

Fitting of the reaction-order and TSB models were carried out using a nonlinear least squares method by minimizing the difference between experimental and calculated values, and the objective function (OF) and fit quality (Fit) were defined as:[2,30,37]

$$OF = \sum ((\frac{d\alpha}{dT})_{\exp} - (\frac{d\alpha}{dT})_{pred})^2 \tag{12}$$

$$Fit(\%) = (1 - \frac{\sqrt{\overline{OF}}}{((\frac{d\alpha}{dT})_{\exp})_{\max}}) \times 100 \tag{13}$$

Where $(\frac{d\alpha}{dT})_{\exp}$ and $(\frac{d\alpha}{dT})_{cal}$ are the experimental and the calculated conversion rates, respectively.

3 Results and discussion

3.1 Physicochemical properties

Table 1 shows the physicochemical properties of the RGE, HRGE, C9PR and HC9PR. According to the GPC analysis, it can clearly be seen that RGE and HRGE are mainly composed of triglycerides, while the molecular weight of RGE is higher

than the HRGE, which is mainly attributed to the fact that part of the RGE has been oxidized in the air.[19-20] This implies that the oxidation stability of HRGE is superior to that of RGE, which is also evidenced by the lower acid value of HRGE. Similarly, hydrogenation of C9PR can obviously reduce the bromine value and improve the oxidation stability. Nevertheless, the softening point of hydrogenated resins is lower than that of unhydrogenated resins because RGE and C9PR are more sensitive to high temperatures thanks to their double bonds.[20] Interestingly, the softening points of RGE and HRGE are higher than those of C9PR and HC9PR respectively, indicating that bio-based resins with good high-temperature stability could be promising alternatives to petro-based resins. Besides, the weight average molecular weight (M_w) and molecular weight distribution (M_w/M_n) between C9PR and HC9PR did not change significantly, indicating that C9PR was stable and did not degrade seriously under mild hydrogenation conditions.[11,24]

3.2 High-temperature stability and pyrolysis kinetics

The pyrolysis behavior and high-temperature stability of the bio-based and petro-based resins were investigated and compared via TG and conversion rate ($d\alpha/dT$) analyses under N_2 atmosphere, and the corresponding results were presented in Fig. 1, table 2 and Fig. S1. A small mass loss is below 500 K, which is attributed to the release of moisture and low volatile matters.[29,38] Remarkably, the RGE and HRGE shows high initial pyrolysis temperature ($T_{5\%}$) of 566 K and 517 K, respectively, while the initial mass-loss step for C9PR and HC9PR respectively starts at 546 K and 477 K, and the similar results are found in T_{peak}, $T_{10\%}$ and $T_{90\%}$, indicating that the

high-temperature stability of bio-based resins is better than that of petro-based resins, which agrees with the results of softening point. The remarkably high thermal stability of bio-based resins may be attributed the highly rigid tricyclic phenanthrene structure.[39-40] This results suggest that bio-based resins have a great potential to replace petro-based resins in environmentally friendly and high-temperature applications.

As shown in table 2, at the same heating rate, the pyrolysis temperature of HRGE with different mass loss is lower than that of RGE, and its maximum conversion rate ($(d\alpha/dT)_{max}$) is also higher than that of RGE, indicating that both the side chain and skeleton structure of HRGE are more readily decomposed than those of RGE due to the highly saturated tricyclic phenanthrene structure. On the other hand, at the same heating rate, there is no significant difference in T_{peak} and $(d\alpha/dT)_{max}$ between C9PR and HC9PR, while the pyrolysis temperatures of HC9PR are lower than those of C9PR at a certain mass loss, revealing that the dominant pyrolysis temperature of the skeleton structures between C9PR and HC9PR is approximately the same, but the weak chemical bonds in HC9PR are more easily cracked. This may be due to the fact that the hydrogenation of C9PR is mainly concentrated in the side chains or heterocyclic rings. Taking into account that the HC9PR was prepared in 200# solvent oil,[11] there was still a small amount of solvent residue despite the vacuum distillation of the product, which would also cause the HC9PR to release more low-volatile matters at low temperatures. Moreover, hydrogenated resins afford lower char residues than unhydrogenated resins. In general, the high-temperature

stability of bio-based and petro-based resins would mildly decrease after hydromodification due to the highly saturated carboncarbon bonds,[20] which is consistent with the results of the softening point.

Notably, the dominating pyrolysis stage for the bio-based and petro-based resins takes place between 500 K and 800 K, with only one significant peak in the pyrolysis curves (see Figs.1 and S1), revealing that the pyrolysis of RGE, HRGE, C9PR and HC9PR may be a single-step reaction.[41] Moreover, the non-isothermal TG and conversion rate peaks would move to the high temperature region with the increase of heating rate due to the thermal hysteresis effect, but the pyrolysis patterns of bio-based and petro-based resins have no changes.[29,33]

In order to further investigate the pyrolysis process of bio-based and petro-based resins, isoconversional model-free and model-fitting methods were adopted to determinate the pyrolysis kinetics model. Firstly, the activation energies (E_α) of various resins are calculated using Friedman and Starink methods based on the linear-regression analysis, as shown in Figs. 2-3 and table 3. Obviously, lower average E_α was observed in C9PR and HC9PR compared with RGE and HRGE, further revealing that the bio-based resins exhibit better high-temperature stability than the petro-based resins. Meanwhile, the mean activation energies of RGE and C9PR are higher than that of HRGE and HC9PR, respectively, further revealing that hydrogenated resins have lower high-temperature stability than unhydrogenated resins. The relationships of activation energies (E_α) and extent of conversions (α) were illustrated in Figs.4. For C9PR and RGE, variations in E_α are not significant, because

the difference between of maximum and minimum activation energies is less than 20% of the mean of E_α value.[31,42] Whereas, for HC9PR and HRGE, a large fluctuations of E_α occurs at α = 0.1 due to the release of more moisture and low-volatile matters, but there are no significant variations in E_α at α = 0.2-0.9. Therefore, the pyrolysis reactions of RGE, HRGE, C9PR and HC9PR in nitrogen atmosphere could be regarded as a single-step reaction, and similar results have been reported in previous work.[30,41-42]

Furthermore, the reaction-order and TSB models were used to evaluate the pyrolysis kinetic parameters of the bio-based and petro-based resins based on the average E_α determined by the differential and integral isoconversional methods, the results were shown in tables 4 and S1. Clearly, the reaction-order model was found to give the best description for the bio-based and petro-based resins pyrolysis mechanism. The qualities of the fitting with the reaction-order model are acceptable for the RGE and C9PR, while slightly worse fitting results are found in HRGE and HC9PR due to the weight losses of moisture and low volatile matters at below 500 K, which are in agreement with the results of TG and model-free analyses. The fitting curves of conversion rate for bio-based and petro-based resins with the reaction-order model at heating rates of 20 $K \cdot min^{-1}$ were shown in Fig. 5.

Considering that moisture has an important effect on the initial weight loss of different resins, a model eliminating the influence of moisture should be considered in order to enhance the fitting results and better reveal the pyrolysis mechanism. The verification experiments were carried out at a heating rate of 20 $K \cdot min^{-1}$ after 2 h

treatment in nitrogen atmosphere at 373 K. The pyrolysis kinetic parameters of bio-based and petro-based resins in the verification experiments were presented in table 5, and the calculated conversion rates were compared with the experimental data as shown in Fig. 6. Notably, the fitting results with the reaction-order model agree well with the experimental data after 373 K pretreatment, revealing that the presence of moisture in different resins would make the activation energy of $\alpha = 0.1$ lower, thus reducing the fitting quality. These results suggest that the reaction-order model is reliable and powerful to fit the pyrolysis reaction of the bio-based and petro-based resins, as well as the moisture in the resins would affect the fitting quality.

3.3 Identification of gaseous products and possible pyrolysis pathways

Based on the above discussion, it was found that the reaction-order model allowed one to describe well the pyrolysis reaction mechanism of bio-based and petro-based resins, however, detail pyrolysis gaseous products information and possible pyrolysis pathways on different resins should be further analyzed using TG-FTIR/MS techniques.

Coupled TG-FTIR experiments were carried out to identify the gas products of bio-based and petro-based resins pyrolysis according to the characteristic absorbance values.[20,29,38,43] The 3D FTIR spectra for the gases released during the bio-based and petro-based resins pyrolysis were continuously recorded in the temperatures range of room temperature to 923 K with a heating rate of 10 $K \cdot min^{-1}$. From Fig.7a-7d, no significant absorbance peaks are found below 500 K, revealing that both bio-based and petro-based resins show highly thermal stability. More impressively, the pyrolysis

of different resins is concentrated in a very narrow temperature range, and there is a highest characteristic absorption peak at about 673 K, further revealing that the pyrolysis of bio-based and petro-based resins is a single-step reaction. These results agree well with the results of TG and kinetics analyses discussed earlier.

Fig. 7e evidently shows the 2D FTIR spectra of volatiles for the bio-based and petro-based resins at 500 K, 673 K and 623 K or 573 K. As shown in Fig. 7e, the characteristic absorbance peaks at the range of 4000-3400 cm^{-1} originate from the release of moisture and alcohols.[20,44] The peaks at the range of 3100-3000 cm^{-1} are corresponded to the asymmetric stretching vibrations of C=C, and the peaks at 1600-1450 cm^{-1} coupled with the signals from 830-650 cm^{-1} are attributed to the aromatic rings.[8,44] Besides, the evident peaks at 3000-2800 cm^{-1} coupled with the signals from 1460 cm^{-1} and 1387 cm^{-1} are attributed to the stretching vibrations of CH, CH_2 and CH_3. The absorbance peaks at 2360 cm^{-1} and 2310 cm^{-1} are assigned to CO_2, and the peak of CO is located at 2180 cm^{-1} and 2110 cm^{-1}, while the distinct peaks at 1900-1650 cm^{-1} are assigned the carbonyl derivatives (e.g. anhydrides, esters, acids, ketones and aldehydes).[20,45] It should be noted that compared with RGE, HRGE does not have two characteristic peaks at 1790 cm^{-1} and 1865 cm^{-1} that are ascribed to anhydrides,[19-20] indicating that the oxidation stability of HRGE is significantly higher than that of RGE, which is consistent with the GPC analysis. Clearly, the intensity and amount of the characteristic absorbance peaks increase significantly with the increase of pyrolysis temperatures. The sharply weak absorbance peaks of O-H stretching vibrations (4000-3400 cm^{-1}), saturated and unsaturated hydrocarbons (3000-2800

cm^{-1}), CO and CO_2 (2400-2100 cm^{-1}, for RGE and HRGE) and olefins (3100-3000 cm^{-1}, for C9PR and HC9PR) are observed in the FTIR spectrum at 500 K, revealing that the molecular structures of bio-based and petro-based resins are outstandingly maintained at 500 K. In addition, the characteristic peak intensities of hydrocarbons of HRGE and HC9PR are more obvious than those of RGE and C9PR, respectively, indicating that the branched chains of hydrogenated resins are decomposed more easily than those of unhydrogenated resins, which is agreement with the results of TG and kinetic analyses. Interestingly, the characteristic peaks of aromatic rings that originate from the pyrolysis of aromatic petro-based resins are first detected at 573 K, while those generated from the pyrolysis of tricyclic phenanthrene structures in bio-based resins are detected at 623 K, indicating that the tricyclic phenanthrene structures of bio-based resins are more difficult to completely crack than the aromatic ring structures of petro-based resins.[3] This results evidently suggest that bio-based resins show better high-temperature stability than petro-based resins, which are consistent with the TG and kinetic results. From the FTIR spectrum at 673 K, the remarkable characteristic peaks of major components are observed, revealing that the molecule structures of bio-based and petro-based resins have been seriously destroyed at 673 K. In short, the main gas products of bio-based resins pyrolysis consist of H_2O, CO, CO_2, CH_4, alcohols and carbonyl derivatives (e.g. esters, acids and aldehydes, ect.), while the main products of petro-based resins pyrolysis are composed of H_2O, CH_4, olefins and aromatic compounds.

Furthermore, coupled TG-MS experiments were performed to further identify the

main components of the gaseous products released from the pyrolysis process of various resins.[8,20] MS spectra monitored at the peak temperatures of 500 K and 673 K were shown in Fig. 8, and the identification of major components of gaseous products were listed in table 6. As shown in Fig. 8, it can be clearly observed that the spectra of different resins at 673 K show more MS signal peaks than those at 500 K, suggesting that the more obvious pyrolysis of major components in the bio-based and petro-based resins occurs at 673 K, which is agreement with the results of TG-FTIR data. Compared with HRGE, RGE exhibits fewer the fragmentation peaks of tricyclic phenanthrene skeletons pyrolysis at 673 K, indicating that the saturated tricyclic phenanthrene structures are more likely to break than unsaturated ones, thus reducing the high-temperature stability of HRGE, which is well supported by the lower pyrolysis temperature and activation energy of HRGE (see tables 2-3). More importantly, at 673 K, some distinct fragment peaks of aromatic compounds are detected in the C9PR and HC9PR, while the weaker fragment peaks of tricyclic phenanthrene structures pyrolysis are detected in the RGE and HRGE, revealing that the tricyclic phenanthrene structure of bio-based resins would require a higher dissociation energy than the aromatic rings of petro-based resins. Therefore, the bio-based resins with thermally stably tricyclic phenanthrene structure have enormous potential for replacing the traditional petro-based resins.

From table 6, for RGE and HRGE, the major components of gaseous products at 500 K are H_2O, CO, CO_2, CH_4, CH_3OH, ethane, propane and isopropanol, and there are new fragmentation peaks of alkenes that come from the pyrolysis of tricyclic

phenanthrene skeletons at 673 K. The major formation of CO, CO_2 and alcohol is attributed to the cracking of carbonyl bonds of carbonyl derivatives (e.g. esters, acids and aldehydes, et al.), and CH_4, C_2H_6 and C_3H_8 are formed because of the cleavage of carboncarbon bonds in the branching chains. Moreover, for C9PR and HC9PR, the major components of gaseous products at 500 K include H_2O, CH_4, CH_3OH, ethene, propane and ethane, and a series of new alkanes and alkenes (such as naphthalene, indene, dicyclopentadiene, methylstyrene and α-methylstyrene, ect.) are formed at 673 K. It is well-known that C9PR is obtained by the polymerization of C9 fraction derived from ethylene cracking in the petro-based industry.[7,10] As a result, a series of C9 alkenes are produced after the thermal depolymerization of C9PR and HC9PR, such as indene, methylstyrene, α-methylstyrene, dicyclopentadiene and naphthalene, et al. The formation of straight-chain alkanes and olefins are mainly due to the cracking of branching chains of C9 alkenes, and the cycloolefins with lower carbon numbers are generated from the cracking and ring-opening reactions of the aromatic and heterocyclic compounds. H_2O mainly originates from the release of moisture, and CH_3OH comes from the cleavage of oxidized resin products.[10-11,19]

Based on the TG-FTIR/MS analyses, the feasible pyrolysis mechanism of bio-based and petro-based resins under non-oxidizing atmosphere was proposed. Since the pyrolysis mechanism of hydrogenated and unhydrogenated resins is similar, only the possible pyrolysis pathways of unhydrogenated resins are discussed in detail in this paper, and the results were shown in Fig. 9. Noticeably, both RGE and C9PR have only one dominating pyrolysis stage, between 500 and 800 K, accompanied by

the cracking of branching chains and the ring-opening reaction of cyclic compounds, and the reaction-order model is found to be the most probable reaction mechanism for various resins pyrolysis. Results from TG-FTIR/MS analysis show it is more difficult to crack the bio-based resin into phenyl than the petroleum-based resin, clearly revealing that the tricyclic phenanthrene structures in the bio-based resins is higher thermally stably structure and require higher pyrolysis temperatures than the cycloaliphatic and aromatic rings in the petro-based resins, and similar results have been reported.[14,17] Before starting pyrolysis, a small amount of compounds is released due to the evaporation of moisture and the cracking of weak chemical bonds, which may reduce the fitting quality of the kinetic model.[41,44] Among them, the cracking of weak chemical bonds of RGE and HRGE consists of the decarboxylation reaction and the cracking of methyl and isopropyl, with concomitant formation of CO, CO_2, CH_3OH, ethane, propane, CH_4 and isopropanol, which is well supported by the results of TG-FTIR/MS analyses. Similarly, the branching chains of C9PR and HC9PR are cracked first to form the straight-chain alkanes and olefins, such as ethane, propane, ethene and propylene. Besides, the weak chemical bonds of hydrogenated resins are more likely to crack than those of unhydrogenated resins, which results in a slight decrease in the high-temperature stability of bio-based and petro-based resins after hydromodification.[20] Therefore, it can be reasonable to conclude that bio-based resins have a great potential to replace petro-based resin in environmentally friendly and high-temperature application.

4.Conclusions

The kinetics and mechanism of RGE, HRGE, C9PR and HC9PR pyrolysis in nitrogen atmosphere were evaluated from the non-isothermal TG data using model-free and model-fitting methods. Activation energy was calculated by Friedman and Starink methods, and the reaction-order model with an empirical function $f(\alpha)=(1-\alpha)^n$ was found to be the most probable reaction mechanism for bio-based and petro-based resins pyrolysis. TG-FTIR/MS results also show that although a small amount of moisture and low volatiles are released before pyrolysis, different resins have only one dominating pyrolysis stage at 500-800 K due to the cracking of branching chain and cyclic compounds. The high-temperature stability of RGE and C9PR will decrease after hydrogenation modification, which is mainly due to the fact that their double bonds are more sensitive to high temperatures. Furthermore, bio-based resins exhibit better high-temperature stability than petro-based resins, which is attributed to the fact that the tricyclic phenanthrene structure of the former is more difficult to completely crack than the cycloaliphatic and aromatic rings of the latter. Moreover, detail pyrolysis gaseous products information were identified based on the TG-FTIR/MS analyses, and the possible pyrolysis pathways of bio-based and petro-based resins were proposed. This investigation shows the bio-based resins with highly stable tricyclic phenanthrene structures are promising substitute for petro-based resins in environmentally friendly and high-temperature application.

Conflicts of interest

There are no conflicts to declare.

Acknowledgments

This work was supported by National Natural Science Foundation of China (Grant Nos. 21878056, 31560241), Guangxi Key Laboratory of Petrochemical Resource Processing and Process Intensification Technology (Grant No. 2019Z002) and Innovation Project of Guangxi Graduate Education (YCBZ2021017).

References

1. Qi Y, Weng Z, Kou Y, Song L, Li J, Wang J, Zhang S, Liu C, Jian X. Synthesize and introduce bio-based aromatic s-triazine in epoxy resin: Enabling extremely high thermal stability, mechanical properties, and flame retardancy to achieve high-performance sustainable polymers. *Chem Eng J*. 2021; 406:126881.
2. Gan YY, Chen WH, Ong HC, Lin YY, Sheen HK, Chang JS, Ling TC. Effect of wet torrefaction on pyrolysis kinetics and conversion of microalgae carbohydrates, proteins, and lipids. *Energ Convers Manage*. 2021; 227:113609.
3. Li Q, Huang X, Liu H, Shang S, Song Z, Song J. Properties enhancement of room temperature vulcanized silicone rubber by rosin modified aminopropyltriethoxysilane as a cross-linking agent. *ACS Sustain Chem Eng*. 2017;5:10002-10010.
4. Chen Y, Xi Z, Zhao L. Curing kinetics of bio-based epoxy resin based on epoxidized soybean oil and green curing agent. *AIChE J*. 2017;63:147-153.
5. Mildenberg R, Zander M, Collin G. Hydrocarbon Resins. New York: John Wiley & Sons, Inc., 2008.
6. Shi J, Zhao P, Fan W, Yang Z, Lin Y, Ouyang J. Facile preparation and application performance evaluation of SBS/C9 petro-based resin blends as modifier for high

viscosity asphalt. *Constr Build Mater.* 2020;262:120073.

7. Jin Z, Zuo X, Long X, Cui Z, Yuan G, Dong Z, Zhang J, Cong Y, Li X. Accelerating the oxidative stabilization of pitch fibers and improving the physical performance of carbon fibers by modifying naphthalene-based mesophase pitch with C9 resin. *J Anal Appl Pyrol.* 2021;154:105009.
8. Liang B, Wang J, Hu J, Li C, Li R, Liu Y, Zeng K, Yang G. TG-MS-FTIR study on pyrolysis behavior of phthalonitrile resin. *Polym Degrad Stability*. 2019:169: 108954.
9. Sun H, Yang J, Zhang H, Yang Q, Wu S, Wang Y, Zhu H,Yue Y, Wang T, Yuan P. Hierarchical Flower-Like NiCu/SiO_2 Bimetallic Catalysts with Enhanced Catalytic Activity and Stability for Petroleum Resin Hydrogenation. *Ind Eng Chem Res*. 2021.
10. Rahmatpour A, Ghasemi Meymandi M. Large-Scale Production of C9 Aromatic Hydrocarbon Resin from the Cracked-petro-based-Derived C9 Fraction: Chemistry, Scalability, and Techno-economic Analysis. *Org Process Res Dev.* 2021;25:120-135.
11. Wu C, Chen X, Tang L, Wei Q, Wei X, Liang J, Wang L. Rationally Constructing A Nano MOF-Derived Ni and CQD Embedded N-Doped Carbon Nanosphere for the Hydrogenation of petro-based Resin at Low Temperature. *ACS Appl Mater Inter.* 2021;13:10855-10869.
12. Yang D, Yang C, Xie J, Wu S, Ye Q, Hu R. Combusting behavior and pyrolysis products evaluation of SARA components separated from bitumen. *Constr Build*

Mater. 2020;244:118401.

13. Zhou D, Wang L, Chen X, Wei X, Liang J, Tang R, Xu Y. Reaction mechanism investigation on the esterification of rosin with glycerol over annealed Fe_3O_4/MOF-5 via kinetics and TGA-FTIR analysis. *Chem Eng J.* 2020;401: 126024.
14. Liu X, Xin W, Zhang J. Rosin-based acid anhydrides as alternatives to petrochemical curing agents. *Green Chem.* 2009;11:1018-1025.
15. Barabde UV, Fulzele SV, Satturwar PM, Dorle AK, Joshi SB. Film coating and biodegradation studies of new rosin derivative. *React Funct polym.* 2005;62: 241-248.
16. Zhang D, Zhou D, Wei X, Liang J, Chen X, Wang L. Green catalytic conversion of hydrogenated rosin to glycerol esters using subcritical CO_2 in water and the associated kinetics. *J Supercrit Fluid.* 2017;125: 12-21.
17. Mustata FR, Tudorachi N. Epoxy resins cross-linked with rosin adduct derivatives. Cross-linking and thermal behaviors. *Ind Eng Chem Res.* 2010;49:12414-12422.
18. Song D, Zhang W, Gupta RK, Melby EG. Role of operating conditions in determining droplet size and viscosity of tackifier emulsions formed via phase inversion. *AIChE J.* 2011;57:96-106.
19. Ren F, Zheng YF, Liu XM, Yue XY, Ma L, Li WG, Lai F, Liu JL, Guan WL. An investigation of the oxidation mechanism of abietic acid using two-dimensional infrared correlation spectroscopy. *J Mol Struct.* 2015;1084:236-243.

20. Mustata F, Tudorachi N. Synthesis and thermal characterization of some hardeners for epoxy resins based on castor oil and cyclic anhydrides. *Ind Crop Prod.* 2021;159:113087.

21. Chu HH, Huang WH, Chuang KS, Shen BH. Adhesion and viscoelastic property of poly (ethylene-co-vinyl acetate) based hot melt adhesives-effects of tackifier and wax. *Int J Adhes Adhes.* 2020;99:102586.

22. Wang J, Lu C, Liu Y, Wang C, Chu F. Preparation and characterization of natural rosin stabilized nanoparticles via miniemulsion polymerization and their pressure-sensitive adhesive applications. *Ind Crop Prod.* 2018;124:244-253.

23. Nong W, Chen X, Wang L, Liang J, Zhong L, Tong Z. non-isothermal decomposition kinetics of abietic acid in argon atmosphere. *Ind Eng Chem Res.* 2011;50:13727-13731.

24. Su D, Chen X, Wei X, Liang J, Tang L, Wang L. Comparison of thermal stability between dicyclopentadiene/hydrogenated dicyclopentadiene petro-based resin: Thermal decomposition characteristics, kinetics and evolved gas analysis by TGA/TG-MS. *Thermochim Acta*. 2021;699:178853.

25. Barrueso-Martínez ML, del Pilar Ferrándiz-Gómez T, Romero-Sánchez MD, Martín-Martínez JM. Characterization of EVA-based adhesives containing different amounts of rosin ester or polyterpene tackifier. *J Adhes.* 2003;79: 805-824.

26. Lee S, Lee K, Kim YW, Shin J. Preparation and characterization of a renewable pressure-sensitive adhesive system derived from ε-decalactone, l-lactide,

epoxidized soybean oil, and rosin ester. *ACS Sustain Chem Eng.* 2015;3:2309-2320.

27. Haluska JL, Riley KL. Hydrogenation process for hydrocarbon resins. US Patent Application US2004/6755963, 2004.
28. Mirabedini SM, Zareanshahraki F, Mannari V.Enhancing thermoplastic road-marking paints performance using sustainable rosin ester. *Prog Org Coat.* 2020;139:105454.
29. Gao R, Zhan L, Guo J, Xu Z. Research of the thermal decomposition mechanism and pyrolysis pathways from macromonomer to small molecule of waste printed circuit board. *J Hazard Mater.* 2020;383:121234.
30. Ali I, Naqvi SR, Bahadar A. Kinetic analysis of Botryococcus braunii pyrolysis using model-free and model fitting methods. *Fuel.* 2018;214:369-380.
31. Vyazovkin S, Burnham AK, Criado JM, Pérez-Maqueda LA, Popescu C, Sbirrazzuoli N. ICTAC Kinetics Committee recommendations for performing kinetic computations on thermal analysis data. *Thermochim Acta.* 2011;520:1-19.
32. Tiwari P, Deo M. Detailed kinetic analysis of oil shale pyrolysis TGA data. *AIChE J*. 2012;58:505-515.
33. Du W, Wang G, Wang Y, Liu X. Thermal degradation of bituminous coal with both model-free and model-fitting methods. *Appl Therm Eng.* 2019;152:169-174.
34. Starink MJ. The determination of activation energy from linear heating rate experiments: a comparison of the accuracy of isoconversion methods. *Thermochim Acta*. 2003;404:163-176.

35. Luo H, Bao LW, Kong LZ, Sun YH. Revealing low temperature microwave-assisted pyrolysis kinetic behaviors and dielectric properties of biomass components. *AIChE J.* 2018; 64:2124-2134.

36. Xiang Z, Liang J, Morgan Jr HM, Liu Y, Mao H, Bu Q. Thermal behavior and kinetic study for co-pyrolysis of lignocellulosic biomass with polyethylene over Cobalt modified ZSM-5 catalyst by thermogravimetric analysis. *Bioresource Technol.* 2018;247:804-811.

37. Bach QV, Chen WH. A comprehensive study on pyrolysis kinetics of microalgal biomass. *Energ Convers Manage*. 2017;131:109-116.

38. Özsin G, Pütün AE. TGA/MS/FT-IR study for kinetic evaluation and evolved gas analysis of a biomass/PVC co-pyrolysis process. *Energ Convers Manage*. 2019;182:143-153.

39. Yan X, Zhai Z, Song Z, Shang S, Rao X. Synthesis and properties of polyester-based polymeric surfactants from diterpenic rosin. *Ind Crop Prod.* 2017;108:371-378;

40. Lin HX, Yang MS, Tian C, Han CR, Song J, Duan JF, Jiang JX, Design of diversified self-assembly systems based on a natural rosin-based tertiary amine for doxorubicin delivery and excellent emulsification. *Colloid Surface B.* 2018; 165:191-198.

41. Shi S, Lei B, Li M, Cui X, Wang X, Fan X, Tand S, Shen J. Thermal decomposition behavior of a thermal protection coating composite with silicone rubber: Experiment and modeling. *Prog Org Coat.* 2020;143:105609.

42. Vyazovkin S, Burnham AK, Favergeon L, Koga N, Moukhina E, Pérez-Maqueda, LA, Sbirrazzuoli N. ICTAC Kinetics Committee recommendations for analysis of multi-step kinetics. *Thermochim Acta.* 2020;178597.

43. Huang J, Liu J, Chen J, Xie W, Kuo J, Lu X, Changa K, Wen S, Sun G, Cai H, Buyukada M, Evrendilek F. Combustion behaviors of spent mushroom substrate using TG-MS and TG-FTIR: thermal conversion, kinetic, thermodynamic and emission analyses. *Bioresource Technol.* 2018;266:389-397.

44. Lu X, Guo H, Que H, Wang D, Liang D, He T, Robin HM, Xu C, Zhang X, Gu X. Pyrolysis mechanism and kinetics of high-performance modified lignin-based epoxy resins. *J Anal Appl Pyrol*. 2021;154:105013.

45. Chrissafis K, Paraskevopoulos KM, Papageorgiou GZ, Bikiaris DN. Thermal decomposition of poly (propylene sebacate) and poly (propylene azelate) biodegradable polyesters: Evaluation of mechanisms using TGA, FTIR and GC/MS. *J Anal Appl Pyrol.* 2011;92:123-130.

Table 1 Physicochemical properties of the RGE, HRGE, C9PR and HC9PR.

Resin	GPC analysis[a]				softening point[b] /K	Acid /bromine value
	M_p	M_w	M_n	M_w/M_n		
RGE	965	1016	950	1.07	410.8	43.7 mg KOH/g[c]
HRGE	825	949	851	1.12	366.8	14.5 mg KOH/g[c]
C9PR	1239	1826	995	1.84	388.4	46.1 g/100 g[d]
HC9PR	1248	1825	1028	1.77	365.7	2.0 g/100 g[d]

[a] Molecular weight distribution was determined by GPC analysis, in which M_p, M_w and Mn are peak-position, weight average and number average molecular weight, respectively.

[b] Softening point determined based on the ASTM-E 28-67 standard.

[c] Acid values determined based on the ASTM D-465 standard.

[d] Bromine value determined by the coulometric method with a bromine valence and bromine index apparatus.

Table 2 The high-temperature stability of bio-based and petro-based resins under N_2 atmosphere.

Resin	Heating rate /K·min^{-1}	$T_{5\%}$[a] /K	T_{peak}[b] /K	$(d\alpha/dT)_{max}$[c] /%·K^{-1}	$T_{10\%}$[a] /K	$T_{90\%}$[a] /K	W_{1053}[d] %
RGE	5	566	671	0.016	607	708	1.15
	10	583	683	0.017	622	706	0.31
	20	600	700	0.015	636	726	0.00
	40	623	711	0.017	652	732	0.48
HRGE	5	517	668	0.021	578	681	0.00
	10	532	681	0.019	590	695	0.03
	20	517	697	0.020	585	704	0.20
	40	542	710	0.020	606	718	0.02
C9PR	5	546	647	0.015	578	666	1.26
	10	568	662	0.016	598	681	1.02
	20	582	675	0.016	611	695	0.70
	40	605	688	0.016	630	709	0.73
HC9PR	5	477	652	0.016	541	673	0.00
	10	496	667	0.016	561	688	0.00
	20	505	679	0.015	577	702	0.00
	40	546	694	0.016	605	718	0.00

[a] $T_{5\%}$, $T_{10\%}$ and $T_{90\%}$: the temperature at which the mass loss is 5%, 10% and 90%, respectively.

[b] T_{peak}- The maximum coversion rate temperature.

[c] $(d\alpha/dT)_{max}$: Maximun conversion rate.

[d] W_{1053}: residual mass at 1053 K.

Table 3 Activation energy (E_α) by the model-free methods.

α	RGE				HRGE				C9PR				HC9PR			
	Friedman		Starink		Friedman		Starink		Friedman		Starink		Friedman		Starink	
	*E*a	R^2	*E*a	R^2	*E*a	R^2	*E*a	R^2	*E*a	R^2	*E*a	R^2	*E*a	R^2	*E*a	R^2
0.10	183.79	1.000	162.14	1.000	141.92	0.992	123.15	0.982	154.74	0.997	134.60	0.999	114.92	0.976	105.68	0.972
0.20	192.22	0.997	175.59	0.998	178.15	0.994	161.64	0.994	167.59	0.993	151.30	0.992	159.59	0.998	145.56	0.991
0.30	193.75	0.988	181.78	0.976	190.81	0.978	172.06	0.977	177.11	0.997	166.54	0.995	169.57	0.993	148.93	0.995
0.40	210.75	0.989	192.06	0.986	193.79	0.996	172.46	0.977	175.29	0.969	165.04	0.975	171.88	0.993	149.51	0.995
0.50	213.28	0.993	189.37	0.998	188.06	0.986	176.74	0.983	170.43	0.992	163.36	0.991	177.59	0.996	163.17	0.992
0.60	215.88	0.981	200.93	0.988	185.41	0.978	178.32	0.981	165.80	0.993	165.01	0.993	159.36	0.993	163.16	0.991
0.70	211.29	0.975	200.95	0.987	191.67	0.989	186.34	0.995	166.40	0.983	164.79	0.992	175.90	0.999	166.85	1.000
0.80	202.40	0.981	200.38	0.992	198.86	0.994	186.43	0.998	171.56	0.994	163.31	0.991	174.23	0.998	163.35	0.992
0.90	207.13	0.914	197.48	0.951	204.37	0.999	181.46	1.000	166.08	0.995	163.26	0.991	175.97	0.993	158.69	0.995
Average	203.39		188.97		185.89		170.95		168.33		159.69		164.33		151.66	

Table 4 Optimized reaction-order model parameters for different resins based on differential and integral isoconversional methods at various heating rates and N_2 atmosphere.

Resin	Heating rate, β /min^{-1}	Differential				Integral-Starink			
		A	n	OF	Fit %	A	n	OF	Fit %
RGE	5	3.09×10^{15}	1.92	5.67×10^{-4}	92.36	1.9×10^{14}	1.74	5.85×10^{-4}	92.24
	10	2.61×10^{15}	1.51	4.28×10^{-4}	93.75	1.76×10^{14}	1.39	3.88×10^{-4}	94.05
	20	2.44×10^{15}	1.58	4.73×10^{-4}	92.79	1.74×10^{14}	1.46	4.69×10^{-4}	92.82
	40	2.33×10^{15}	1.41	2.47×10^{-4}	95.25	1.76×10^{14}	1.29	2.69×10^{-4}	95.04
HRGE	5	1.19×10^{14}	1.06	1.08×10^{-3}	91.76	6.64×10^{12}	0.92	9.71×10^{-4}	92.20
	10	1.23×10^{14}	1.05	8.56×10^{-4}	92.14	7.22×10^{12}	0.90	6.90×10^{-4}	92.94
	20	9.84×10^{13}	0.89	8.54×10^{-4}	92.37	6.23×10^{12}	0.76	1.71×10^{-3}	90.95
	40	9.35×10^{13}	0.77	8.14×10^{-4}	94.11	6.30×10^{12}	0.65	1.65×10^{-3}	91.61
C9PR	5	1.51×10^{13}	1.29	3.54×10^{-4}	93.96	2.68×10^{12}	1.21	3.28×10^{-4}	94.18
	10	1.28×10^{13}	1.22	2.29×10^{-4}	94.99	2.39×10^{12}	1.14	3.88×10^{-4}	93.47
	20	1.33×10^{13}	1.21	1.99×10^{-4}	95.33	2.56×10^{12}	1.13	2.25×10^{-4}	95.03
	40	1.37×10^{13}	1.17	2.35×10^{-4}	94.92	2.74×10^{12}	1.10	2.63×10^{-4}	94.63
HC9PR	5	6.10×10^{12}	1.51	1.62×10^{-3}	86.67	4.73×10^{11}	1.35	1.14×10^{-4}	88.82
	10	5.35×10^{12}	1.40	1.33×10^{-3}	87.91	4.41×10^{11}	1.25	9.07×10^{-4}	90.02
	20	5.31×10^{12}	1.34	9.17×10^{-4}	89.96	4.62×10^{11}	1.19	6.20×10^{-4}	91.30
	40	5.00×10^{12}	1.36	6.13×10^{-4}	91.70	4.67×10^{11}	1.22	4.73×10^{-4}	92.70

Table 5 Optimized reaction-order model parameters of different resins based on differentialand integral isoconversional methods at a heating rate of 20 $K \cdot min^{-1}$ after 2 h treatment in nitrogen atmosphere at 373K.

Resin	Differential				Integral			
	A	n	OF	Fit %	A	n	OF	Fit %
RGE	2.41×10^{15}	0.91	4.63×10^{-4}	95.54	1.70×10^{14}	0.80	4.50×10^{-4}	95.60
HRGE	9.21×10^{13}	0.82	4.29×10^{-4}	95.71	5.91×10^{12}	0.70	5.69×10^{-4}	95.06
C9PR	1.46×10^{13}	1.30	1.89×10^{-4}	95.44	2.80×10^{12}	1.22	1.76×10^{-4}	96.37
HC9PR	4.28×10^{12}	1.23	4.77×10^{-4}	94.01	3.83×10^{12}	1.09	3.33×10^{-4}	95.00

Table 6 Identification of main components in the gaseous products released from the RGE, HRGE, and C9PR and HC9PR pyrolysis.

Resin	MS signals	Molecular formula/ weight	Compound
RGE and HRGE	18,17	H_2O/18	Water
	16,15,14,13,12	CH_4/16	Methane
	30, 27, 26	C_2H_6	Ethane
	44,28,16,12	CO_2	CO_2
	28,16,12	CO	CO
	32,31,30,29	CH_4O/32	Methanol
	44,43,42,41,40,39,30,29,28,27,26	C_3H_8/43	Propane /isopropane
	56,55,32,31,30,29,27,26,25	C_3H_4O	Propyl alcohol
	133,131,121,119,105,91,81,79,77,	$C_{10}H_{13}$/133	Bicyclic [4,4,0]-2,4- decadiene,
	67,55,53,52,51,28,25,14,12	$C_{10}H_{11}$/131	Bicyclic [4,4,0] -2-decene
C9PR and HC9PR	18,17	H_2O/18	Water
	16,15,14,13,12	CH_4/16	Methane
	32,31,30,29	CH_4O/32	Methanol
	28,27,26	C_2H_4	Ethene
	42,41,39,28,27,26	C_3H_6/42	Propylene
	30, 29, 15,14	C_2H_6	Ethane
	44,43,42,41,29,28,27,26	C_3H_8/44	Propane
	58, 57,43,42,29,28,27,26	C_4H_{10}/58	Butane
	91,89,77,65,63,51,39,28,27,12	C_7H_7/91	Benzyl group, tropyllium ion
	132,66,65	$C_{10}H_{12}$/132	Dicyclopentadiene
	130,129,115	$C_{10}H_{10}$/130	1-Methylindene, 2-Methyl-1H-indene
	128,127	$C_{10}H_8$/128	Naphthalene
	120,119,92,91,77,75,63,43,15	C_9H_{12}/120	Trimethylbenzene, n-propylbenzene, isopropylbenzene
	118,117,105,91,92,89,77,65,63,41	C_9H_{10}/118	Methylstyrene, α-methylstyrene, allylbenzene, 1-ethyl-2-methylbenzene, 3-ethyltoluene, 4-ethyltoluene
	116,115,114	C_9H_8/116	Indene
	106,105,91,77,76,65,15	C_8H_{10}/106	O-xylene, ethylbenzene
	104,103,77,27	C_8H_9/105	Styrene
	134,105,92,91,77,57,65	$C_{10}H_{14}$/134	n-Butylbenzene

Figure Captions

Fig. 1 TG curves of RGE (a), HRGE (b), C9PR (c) and HC9PR (d) at 5, 10, 20 and 40 $K \cdot min^{-1}$ in N_2 atmosphere.

Fig. 2 Isoconversional plots of Friedman method for RGE (a), HRGE (b), C9PR (c) and HC9PR (d) pyrolysis.

Fig. 3 Isoconversional plots of Starink method for RGE (a), HRGE (b), C9PR (c) and HC9PR (d) pyrolysis.

Fig. 4 Relationship between activation energy and extent of conversion.

Fig. 5 Fitting curves of conversion rate of different resins with the reaction-order model at heating rates of 20 $K \cdot min^{-1}$. (a) RGE, (b) HRGE, (c) C9PR and (d) HC9PR.

Fig. 6 Fitting curves of conversion rate of different resins with the reaction-order model at heating rates of 20 $K \cdot min^{-1}$ after 2 h treatment in nitrogen atmosphere at 373K. (a) RGE, (b) HRGE, (c) C9PR and (d) HC9PR.

Fig. 7 TG-FTIR analyses of bio-based and petro-based resins pyrolysis with a heating rate of 10 $K \cdot min^{-1}$. 3D FTIR diagrams of RGE (a), HRGE (b),C9PR (c) and HC9PR (d), and FTIR spectra of volatiles at different temperatures (e).

Fig. 8 MS spectra of the gaseous products for bio-based and petro-based resins pyrolysis at 500 K and 673 K with the heating rate of 10 $K \cdot min^{-1}$.

Fig. 9 The possible pyrolysis pathways of RGE and C9PR under non-oxidizing atmosphere.

Fig. 1

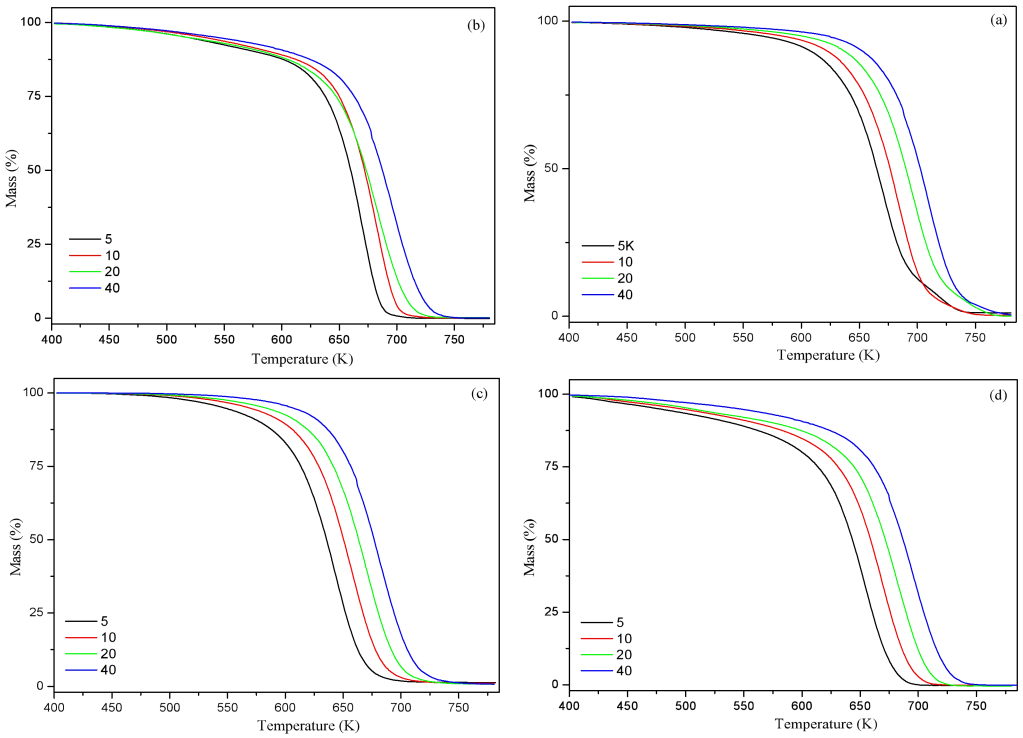
(b)
Mass (%)
Temperature (K)
5
10
20
40
(a)
5K
10
20
40
(c)
(d)

Fig. 2

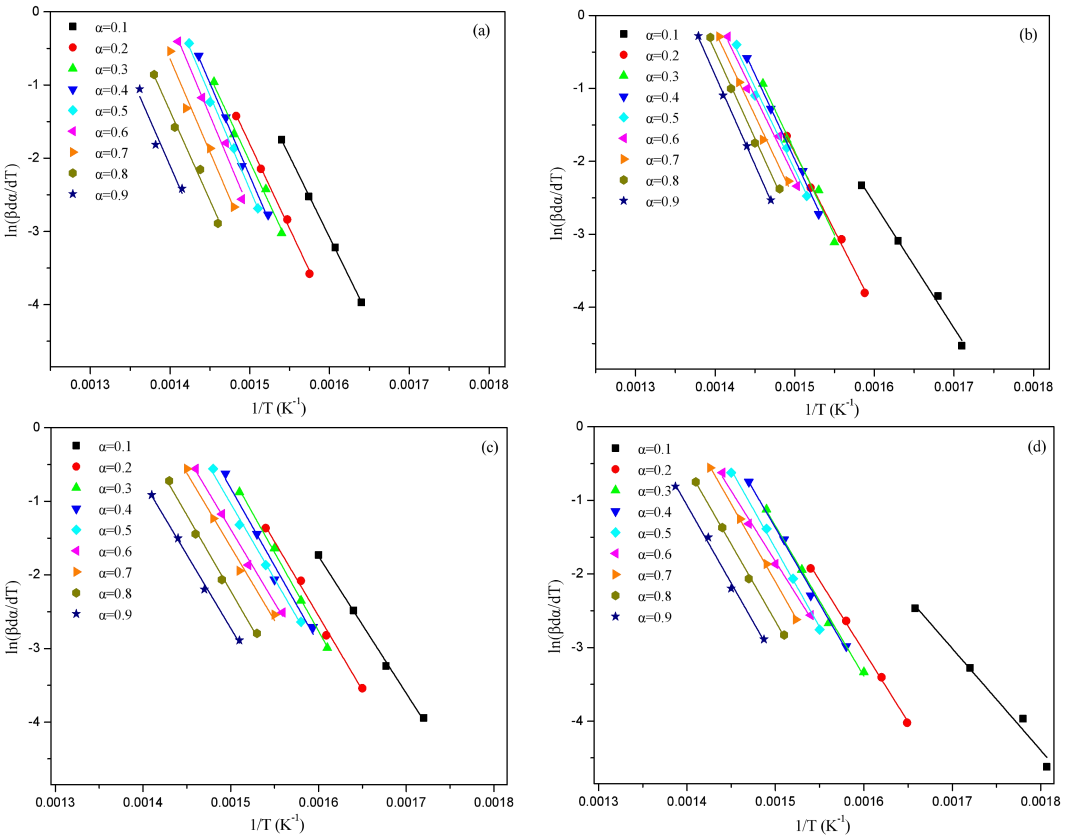
(a)
ln(βdα/dT)
1/T (K-1)
α=0.1
α=0.2
α=0.3
α=0.4
α=0.5
α=0.6
α=0.7
α=0.8
α=0.9
(b)
(c)
(d)

Fig. 3

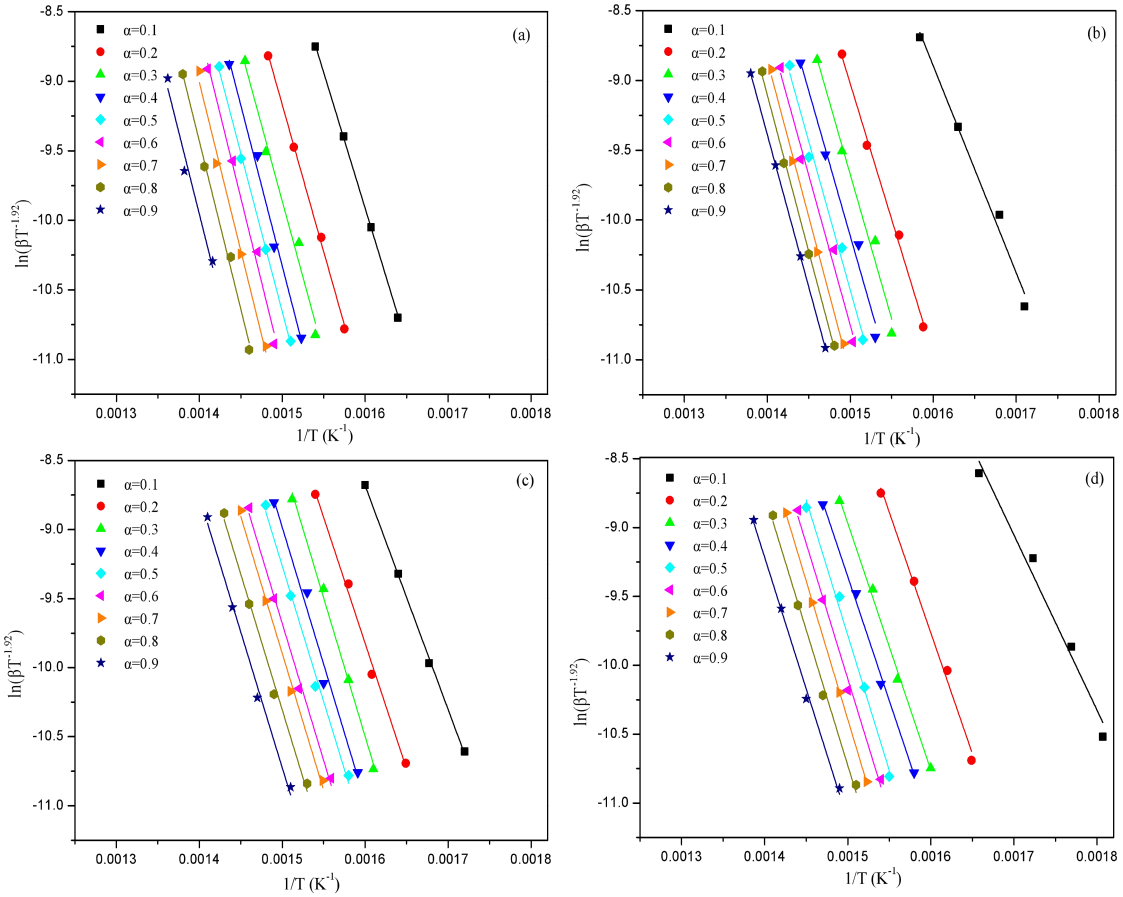
(a)
(b)
(c)
(d)
α=0.1
α=0.2
α=0.3
α=0.4
α=0.5
α=0.6
α=0.7
α=0.8
α=0.9
ln(βT^-1.92)
1/T (K^-1)
-8.5
-9.0
-9.5
-10.0
-10.5
-11.0
0.0013
0.0014
0.0015
0.0016
0.0017
0.0018

Fig. 4

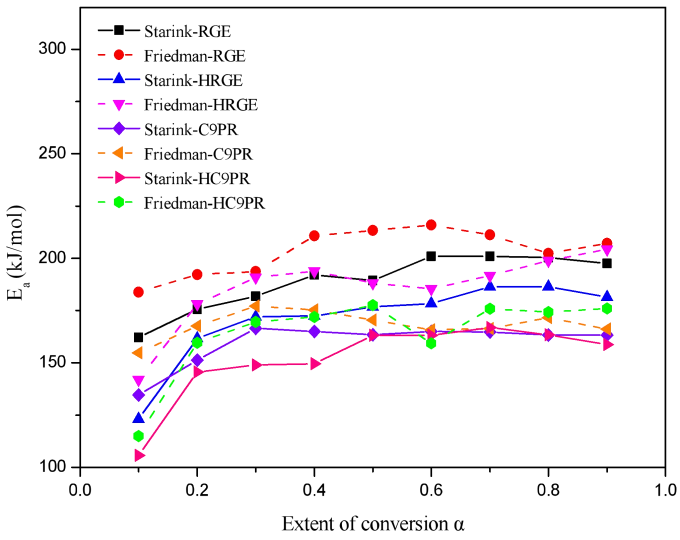
Starink-RGE
Friedman-RGE
Starink-HRGE
Friedman-HRGE
Starink-C9PR
Friedman-C9PR
Starink-HC9PR
Friedman-HC9PR
E_a (kJ/mol)
Extent of conversion α
300
250
200
150
100
0.0
0.2
0.4
0.6
0.8
1.0

Fig. 5

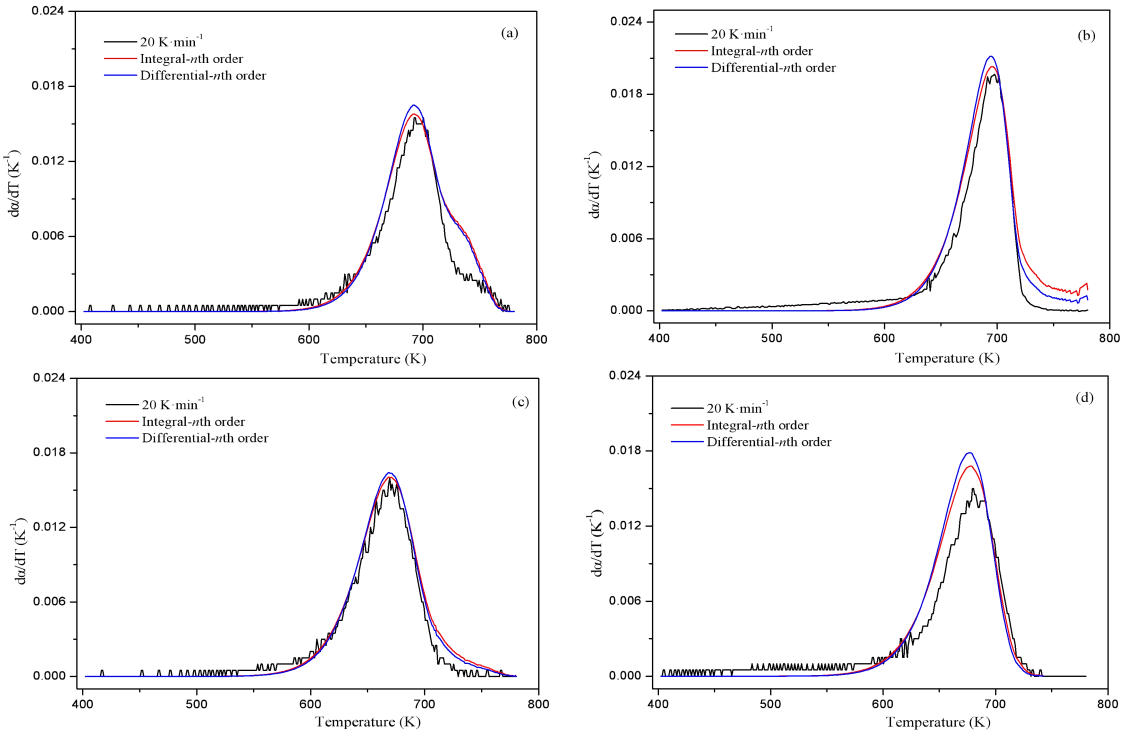
(a)
(b)
(c)
(d)
20 K·min-1
Integral-nth order
Differential-nth order
dα/dT (K-1)
Temperature (K)

Fig. 6

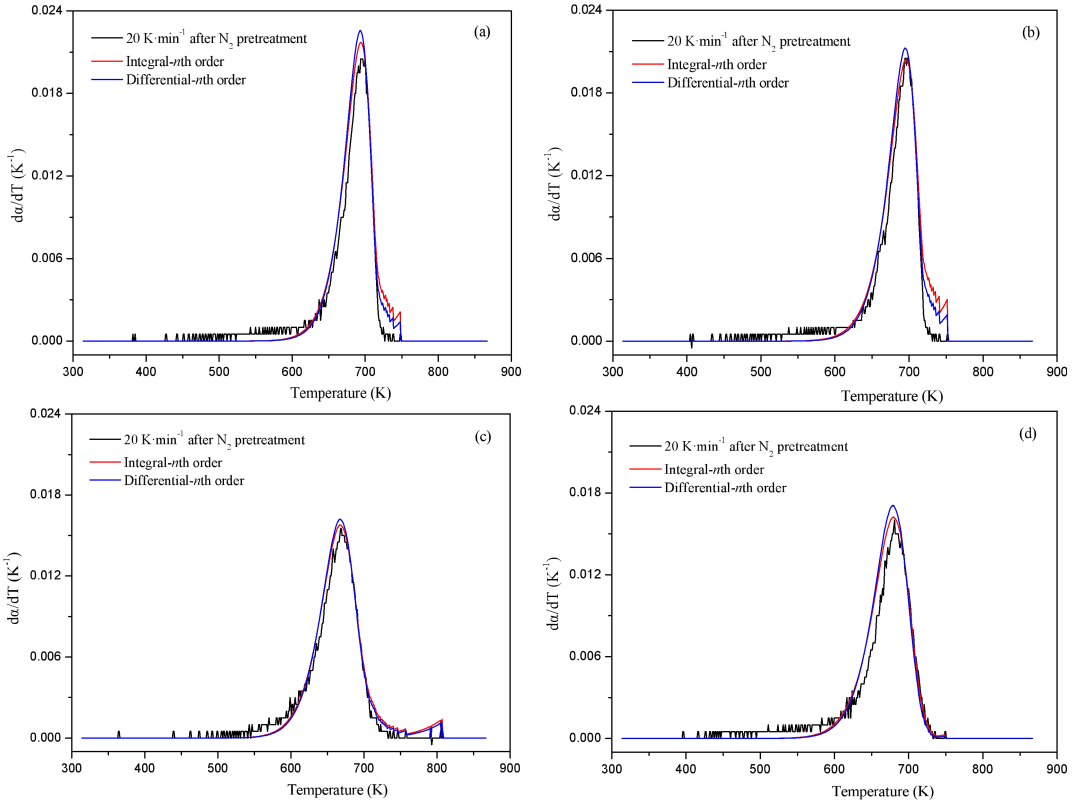
(a)
(b)
(c)
(d)
20 K·min-1 after N2 pretreatment
Integral-nth order
Differential-nth order
dα/dT (K-1)
Temperature (K)

Fig. 7

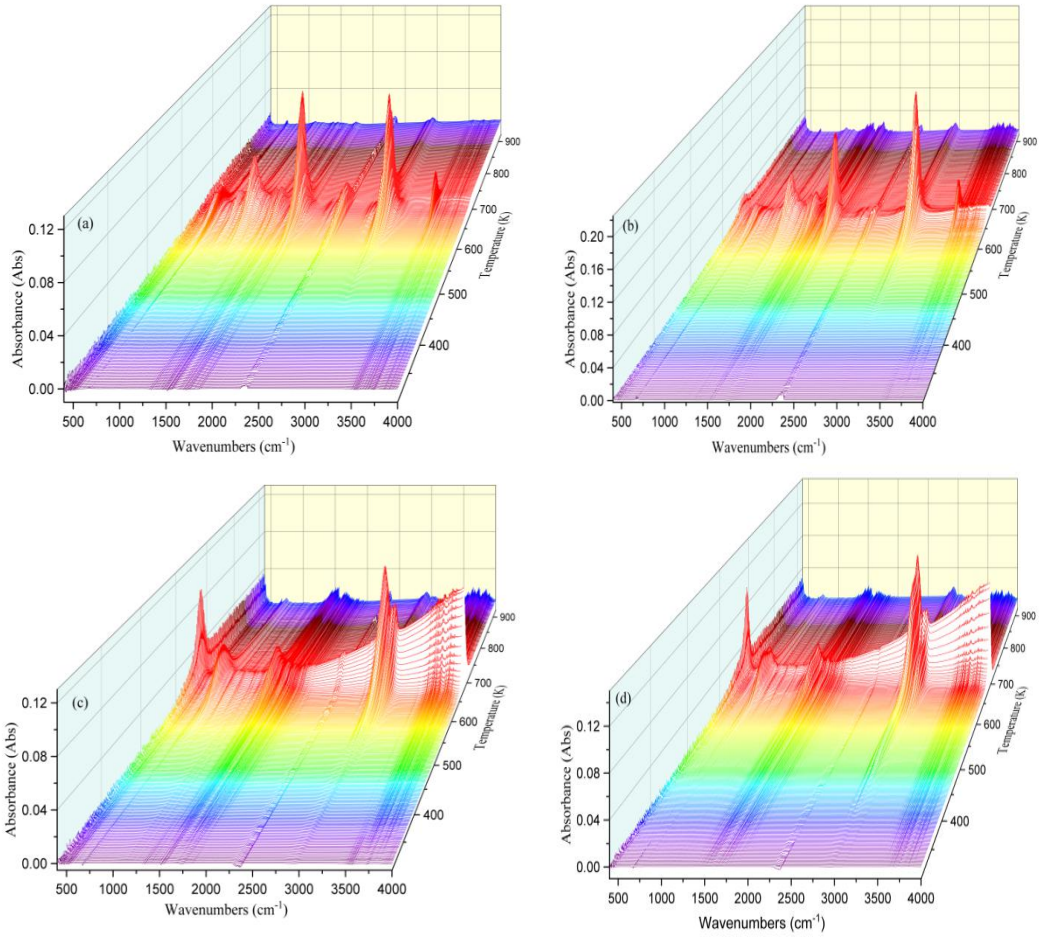
(a)
(b)
(c)
(d)
Absorbance (Abs)
Wavenumbers (cm-1)
Temperature (K)

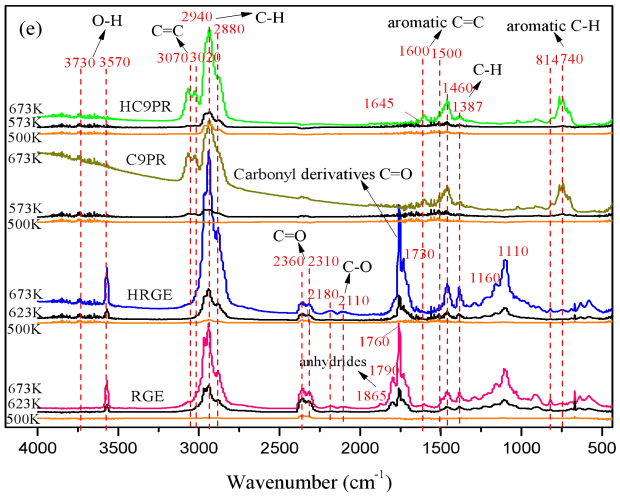
(e)
O-H
C=C
C-H
aromatic C=C
aromatic C-H
3730 3570
3070 3020
2940
2880
1600 1500
1460
1387
1645
814 740
HC9PR
C9PR
Carbonyl derivatives C=O
C=O
2360 2310
C-O
2180 2110
1730
1110
1160
HRGE
anhydrides
1760
1790
1865
RGE
673K
623K
573K
500K
Wavenumber (cm-1)

Fig. 8

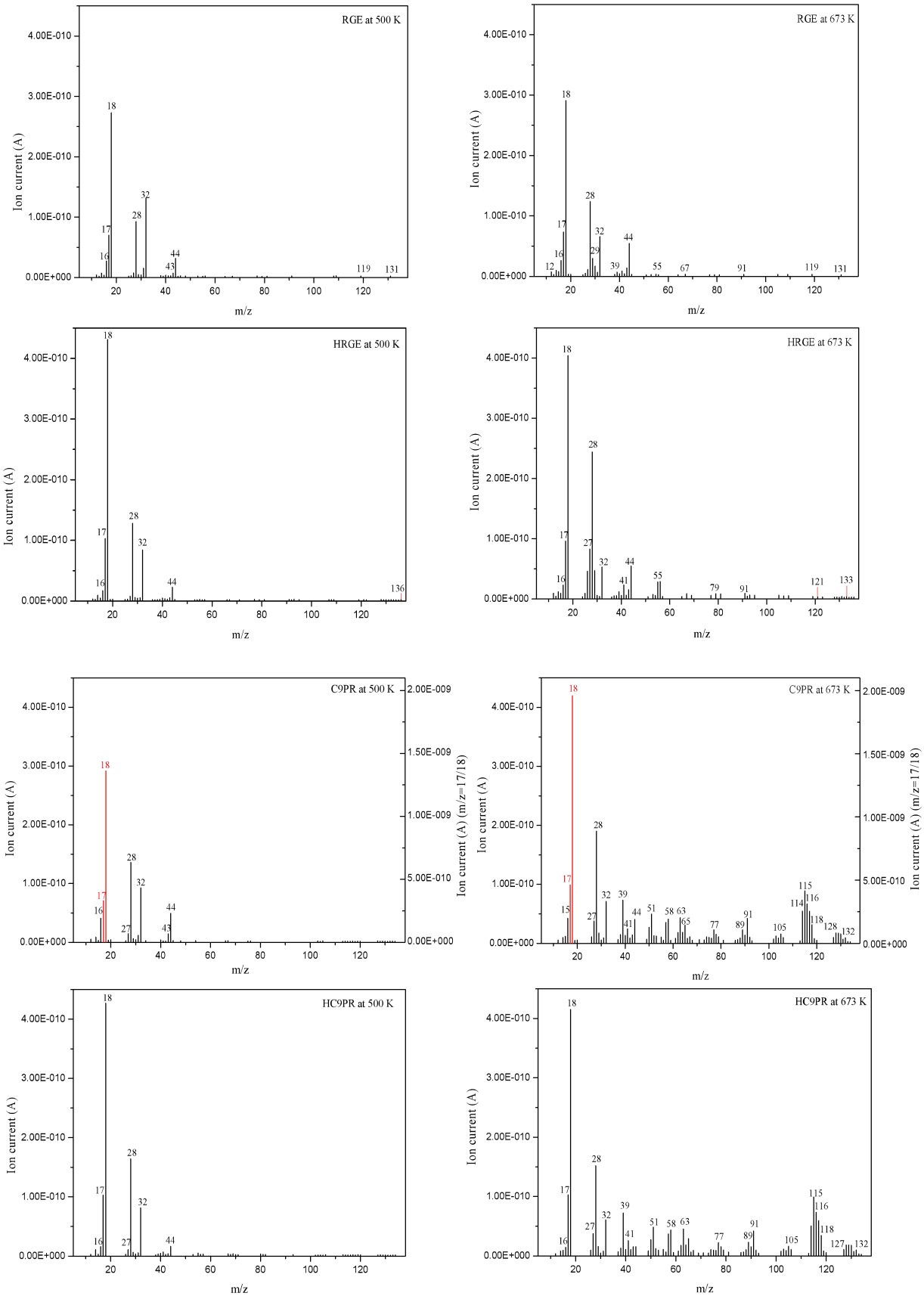
RGE at 500 K
RGE at 673 K
HRGE at 500 K
HRGE at 673 K
C9PR at 500 K
C9PR at 673 K
HC9PR at 500 K
HC9PR at 673 K
Ion current (A)
Ion current (A) (m/z=17/18)
m/z

Fig. 9

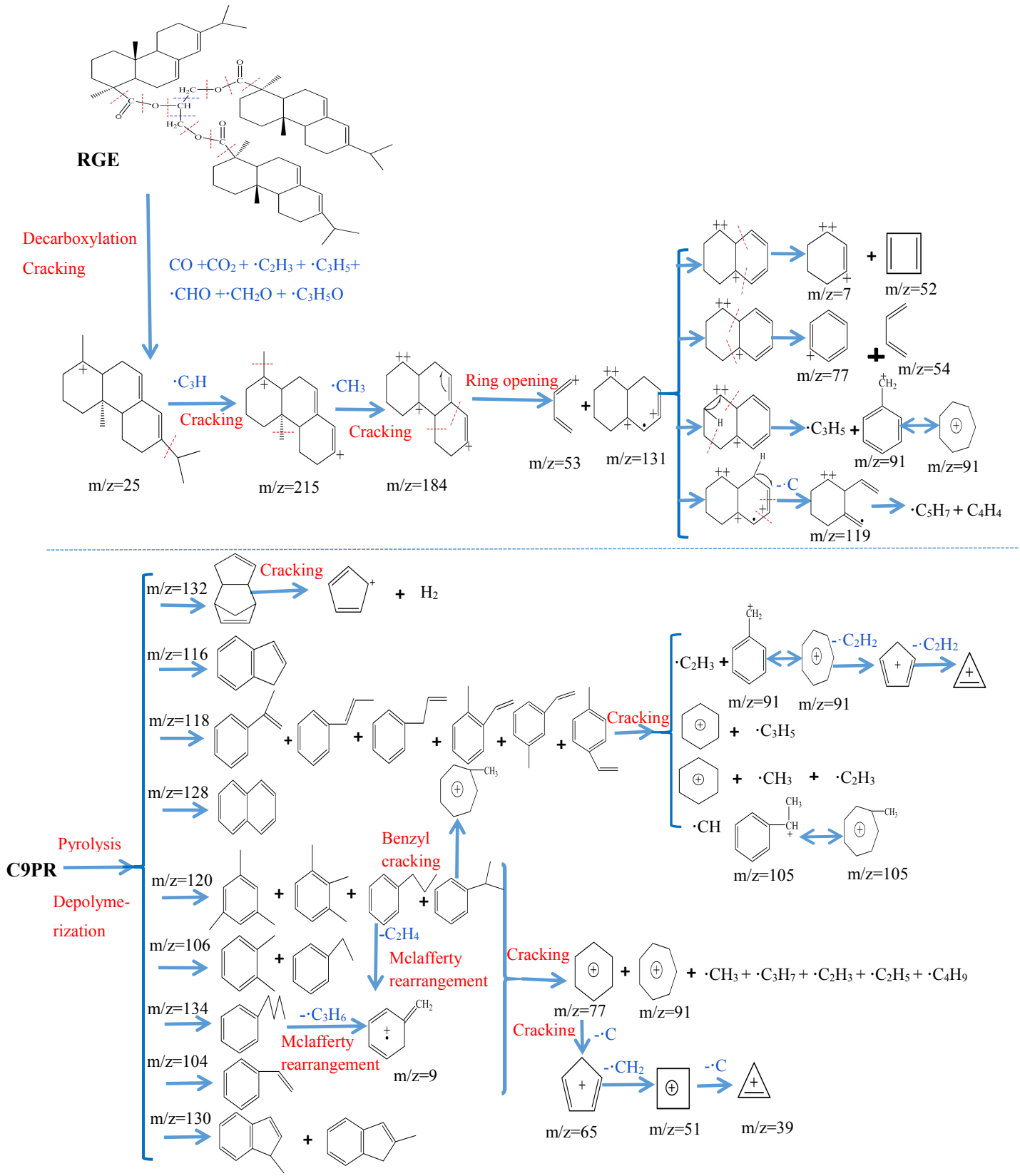
RGE
Decarboxylation
Cracking
CO +CO2 + ·C2H3 + ·C3H5+
·CHO +·CH2O + ·C3H5O
·C3H
Cracking
·CH3
Cracking
Ring opening
m/z=25
m/z=215
m/z=184
m/z=53
m/z=131
m/z=7
m/z=52
m/z=77
m/z=54
·C3H5 +
m/z=91
m/z=91
-·C
·C5H7 + C4H4
m/z=119
Pyrolysis
C9PR
Depolyme-
rization
m/z=132
Cracking
+ H2
m/z=116
m/z=118
m/z=128
m/z=120
m/z=106
m/z=134
m/z=104
m/z=130
Benzyl
cracking
-C2H4
Mclafferty
rearrangement
-·C3H6
Mclafferty
rearrangement
m/z=9
Cracking
·C2H3 +
-·C2H2
-·C2H2
m/z=91
m/z=91
·C3H5
·CH3 + ·C2H3
·CH
m/z=105
m/z=105
Cracking
+ ·CH3 + ·C3H7 + ·C2H3 + ·C2H5 + ·C4H9
m/z=77
m/z=91
Cracking
-·C
-·CH2
-·C
m/z=65
m/z=51
m/z=39